



Contents lists available at ScienceDirect

Journal of Alloys and Compounds

journal homepage: <http://www.elsevier.com/locate/jalcom>



Synthesis, structural and spectroscopic properties of orthorhombic compounds BaLnCuS₃ (Ln = Pr, Sm)

Nikita O. Azarapin ^a, Aleksandr S. Aleksandrovsky ^{b,c}, Victor V. Atuchin ^{d,e,f,*}, Tatyana A. Gavrilova ^g, Aleksandr S. Krylov ^h, Maxim S. Molokeev ^{i,j,k}, Shaibal Mukherjee ^l, Aleksandr S. Oreshonkov ^{h,k}, Oleg V. Andreev ^a

^a Institute of Chemistry, Tyumen State University, Tyumen, 625003, Russia

^b Laboratory of Coherent Optics, Kirensky Institute of Physics Federal Research Center KSC SB RAS, Krasnoyarsk, 660036, Russia

^c Department of Photonics and Laser Technologies, Siberian Federal University, Krasnoyarsk, 660041, Russia

^d Laboratory of Optical Materials and Structures, Institute of Semiconductor Physics, SB RAS, Novosibirsk, 630090, Russia

^e Functional Electronics Laboratory, Tomsk State University, Tomsk, 634050, Russia

^f Research and Development Department, Kemerovo State University, Kemerovo, 650000, Russia

^g Laboratory of Nanodiagnosis and Nanolithography, Institute of Semiconductor Physics, SB RAS, Novosibirsk, 630090, Russia

^h Laboratory of Molecular Spectroscopy, Kirensky Institute of Physics Federal Research Center KSC SB RAS, Krasnoyarsk, 660036, Russia

ⁱ Laboratory of Crystal Physics, Kirensky Institute of Physics Federal Research Center KSC SB RAS, Krasnoyarsk, 660036, Russia

^j Department of Physics, Far Eastern State Transport University, Khabarovsk, 680021, Russia

^k Siberian Federal University, Krasnoyarsk, 660079, Russia

^l Hybrid Nanodevice Research Group (HNRG), Electrical Engineering, Indian Institute of Technology Indore, Madhya Pradesh, 453552, India

ARTICLE INFO

Article history:

Received 2 September 2019

Received in revised form

20 November 2019

Accepted 20 November 2019

Available online 23 November 2019

Keywords:

Complex sulfides

Crystal structure

SEM

Raman

ABSTRACT

Ternary sulfides BaPrCuS₃ and BaSmCuS₃ are first synthesized by the sulphidation reaction of a mixture of related oxides and metal Cu in a flow of (CS₂, H₂S) at 1170 K. The crystal structures of BaPrCuS₃ and BaSmCuS₃ are obtained by Rietveld method. BaPrCuS₃ crystallizes in space group *Pnma* with unit cell parameters $a = 10.56074(6)$, $b = 4.11305(2)$ and $c = 13.42845(7)$ Å, $V = 583.289(5)$ Å³, $Z = 2$ (structure type Eu₂CuS₃). BaSmCuS₃ crystallizes in space group *Cmcm* with unit cell parameters $a = 4.07269(4)$, $b = 13.4499(1)$ and $c = 10.3704(1)$ Å, $V = 568.06(1)$ Å³, $Z = 2$ (structure type KZrCuS₃). The structural model is proposed for the *Cmcm* → *Pnma* transition in ABCX₃ (X = S, Se) compounds for the sequence Sm-Pm-Nd-Pr. The dimensionless tolerance factor $t = \text{IR}(A) \times \text{IR}(C)/\text{IR}(B)^2$ is suggested to control the boundary between the *Cmcm* and *Pnma* structures. The micromorphological, thermal and spectroscopic properties are evaluated for BaPrCuS₃. The compound melts incongruently at $T_{\text{melt}} = 1580.9$ K. In BaPrCuS₃, the band gap is estimated to be 2.1 eV. The vibrational parameters of BaPrCuS₃ and BaSmCuS₃ are comparatively observed by Raman spectroscopy.

© 2019 Published by Elsevier B.V.

1. Introduction

Complex chalcogenide compounds have interesting chemical and physical properties and the materials are widely used in modern optical and electronic technologies [1–10]. For the recent years, complex Cu⁺-containing sulfides and selenides have been considered as promising thin film absorber materials in solar cell structures [11–16]. This activated general interest to crystal

chemistry and the properties of Cu⁺ chalcogenides, including a search for new materials. In particular, the compounds with generalized composition ABCX₃, where A – alkaline-earth metal, B – d- or f-element, C – other d-element and X – chalcogenide, can be considered [1]. Earlier, besides crystal structures, the semiconductor, magnetic, optical and thermodynamic properties were reported on for the selected compounds from this family [1,17–25]. Besides, several Eu²⁺BCS₃ compounds have been recently discovered [7,26–28]. It is known that ABCX₃ compounds can crystallize in seven structural types: KZrCuS₃ (*Cmcm*), Eu₂CuS₃ (*Pnma*), Ba₂MnS₃ (*Pnma*), BaCuLaS₃ (*Pnma*), BaAgErS₃ (*C2/m*), NaCuTiS₃ (*Pnma*) and TlCuTiTe₃ (*P2₁/m*) [1]. Among these crystals, the

* Corresponding author. Institute of Semiconductor Physics, Novosibirsk, 630090, Russia.

E-mail address: atuchin@thermo.isp.nsc.ru (V.V. Atuchin).

Al_nCuQ₃ compounds are particularly interesting because Ln elements have rich crystal chemistry and specific spectroscopic properties.

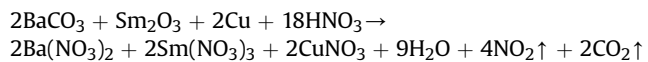
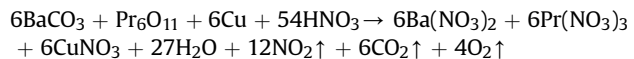
The known ALnCuS₃ compounds crystallize in Eu₂CuS₃ (*Pnma*) or KZrCuS₃ (*Cmcm*) structural types, and the rules governing the relation between the element composition and structure type were not defined for this ternary sulfide family [1]. The crystal structures related to these structural types are very similar. The structures are formed by the layers of CuX₄ tetrahedra and LnX₆ octahedra [29,30]. The present study is aimed at the synthesis and evaluation of compounds BaPrCuS₃ and BaSmCuS₃ as the representative members of ALnCuS₃ sulfides. The compounds were not observed earlier. As to other BaLnCuS₃ sulfides, several compounds were synthesized in the past for Ln = La, Ce, Nd, Er, Sc, Y and the structures were defined for BaLaCuS₃ (*Pnma*) and BaErCuS₃ (*Cmcm*) [17,18]. Also, the space groups *Pnma* and *Cmcm* were adopted for the compounds containing Ln = Ce, Nd and Ln = Sc, Y, Gd, respectively. Thus, the phase transition appears on the rare-earth element substitution in BaLnCuS₃ structures. The formation of BaCuLnS₃ (Ln = Pr, Sm) is assumed in quasiterinary BaS-Ln₂S₃-Cu₂S systems. It should be mentioned that the BaS-Ln₂S₃-Cu₂S phase diagrams have not been defined yet for Ln = Pr, Sm. The known analogous systems (Ba,Sr,Eu²⁺)S-Ln₂S₃-Cu₂S have the composite equilibria including peritectic/eutectic interactions and extensive ranges of solid solutions [22,23,28,31,32] and, respectively, the synthesis of BaPrCuS₃ and BaSmCuS₃ seems to be not trivial. In the present experiment, the sulfides are prepared by the sulphidation method and final powder products are observed by conventional experimental techniques to see their structural, morphological and vibrational characteristics.

2. Experimental section

Syntheses. BaPrCuS₃ and BaSmCuS₃ compounds were prepared in powder forms by the sulphidation of oxide mixtures obtained after the decomposition of metal nitrate solutions. In the synthesis, for better comparison, the key steps were the same for both compounds of barium, rare-earth element and copper.

The following high purity starting reagents were used: Cu (99.9%, SZB Tsvetmet, Russia), BaCO₃ (99.99%, ultrapure, KAI YONG, China), Pr₆O₁₁ (99.99%, ultrapure, TDM-96 Ltd. Russia), Sm₂O₃ (99.99%, ultrapure, TDM-96 Ltd. Russia) and concentrated nitric acid solution (C(HNO₃) = 0.0146 mol/m³, ultrapure, Vekton Ltd., Russia). Ammonium rhodanide NH₄SCN (98%, Vekton Ltd., Russia). Weighing them was carried out on the analytical balance Mettler Toledo with the accuracy of 0.1 mg. Before weighing, a ~1 mm thick copper plate was etched in the HClO₃ solution to remove the surface oxide and was washed out in distilled water. Then, the Cu plate was cut into segments with an area ~1–5 mm². All starting metal oxides were being calcined in quartz crucibles at 1300 K for 5 h in the air to remove surface adsorbates and decompose the hydrocarbonates commonly present on the rare-earth oxide surface. The acid solutions were measured by means of glass measuring graduates with the accuracy of 0.1 cm³.

For the synthesis of BaPrCuS₃, the starting reagents were taken at the stoichiometric molar ratio 6Cu: Pr₆O₁₁: 6BaCO₃ (Cu – 0.8151 g, Pr₆O₁₁ – 2.1866 g, BaCO₃ – 2.5289 g). For BaSmCuS₃, the starting reagents were taken at the stoichiometric molar ratio 2Cu:Sm₂O₃:2BaCO₃ (Cu – 0.7967 g, Sm₂O₃ – 2.1832 g, BaCO₃ – 2.4718 g). The charge was inserted in a heat-resistant flat-bottom beaker and, then, 10 cm³ of concentrated HNO₃ (~21% excess) was added. For the best dissolution, the mixture was warmed up on a laboratory tile for the total disappearance of solid components. The solutions of initial nitrates were formed by reactions:



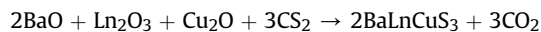
Then, the temperature was increased to 500–600 K and the solution was evaporated up to the formation of a solid. Upon the heating, the solution color changed from blue to green and the brown gas (NO₂) appeared. That indicates the formation of a compound or a complex on the basis of Cu. The high temperature was kept up to the evaporation of all volatile components. As a result of this treatment, a black cake was formed. After the evaporation stage, the beaker was cooled and the cake was extracted. Then, the solid cake was ground in an agate mortar. The powder was inserted in a quartz boat and treated in the muffle furnace at 1170 K until the end of residual brown gas extraction. After this moment, the sample was calcinated at 1170 K for 2 h in the air. After the annealing, the quartz boat was cooled to room temperature and the final product was ground in an agate mortar. As a result, the stoichiometric oxide mixture was formed.

The sulphidation process was carried out in a vertical quartz reactor at the temperature of 1270 K. The oxide charge was placed in a silica container and inserted in the reactor. Then the reactor was heated to 1270 K and filled with a mixture of argon and sulphiding gas CS₂/H₂S generated by the decomposition of ammonium thiocyanate NH₄CSN [33]. For each substance, the reaction was



Fig. 1. Photo of (a) BaPrCuS₃ and (b) BaSmCuS₃ samples.

being carried out for 5 h:



The final powder products of BaLnCuS_3 were of flavovirent color, as shown in Fig. 1. As it appears, the color similarity of the compounds is dominated by the presence of Cu^+ . The following advantages of this synthesis route could be mentioned:

- sedimentation from the nitrate solution allows for the sample homogenization that reduces the time needed for the synthesis of oxide precursor and increases the final product yield.
- less time needed for the synthesis of sulfide compound in comparison with that typical of ampule synthesis methods.
- oxide precursors stable at normal conditions are used in the sulfide synthesis.

Characterization. The powder diffraction data of BaLnCuS_3 for Rietveld analysis were collected at room temperature with a Bruker D8 ADVANCE powder diffractometer ($\text{Cu-K}\alpha$ radiation) and linear VANTEC detector. The step size of 2θ was 0.016° . The 2θ range of $10\text{--}70^\circ$ was measured with a 0.6 mm divergence slit and the counting time was 7 s per step, but the 2θ range of $70\text{--}150^\circ$ was measured with a 2 mm divergence slit and 12 s per step. Larger slits allow for a noticeable increase of the intensity of high-angle peaks without a loss of resolution because the high-angle peaks are broad enough to be not affected by a bigger divergence beam. The esd's $\sigma(I_i)$ of all points on the patterns were calculated using intensities I_i : $\sigma(I_i) = I_i^{1/2}$. The intensities and obtained esd's were further normalized: $I_{i,\text{norm}} = I_i \times 0.6 \times 7/(\text{slit width} \times \text{time per step})$, $\sigma_{\text{norm}}(I_i) = \sigma(I_i) \times 0.6 \times 7/(\text{slit width} \times \text{time per step})$, taking into account the actual divergence slit width value, which was used to measure each particular intensity I_i , and saved in the xye-type file. So, the transformed powder pattern has a usual view in the whole 2θ range of $5\text{--}150^\circ$, but all high-angle points have small esd values.

The optical absorption measurements were carried out with the use of a UV-2600 Series Shimadzu spectrometer using BaSO_4 as a reference sample, with the powder samples of materials under investigation placed in a 0.16 mL Powdered Sample Holder, at room temperature. The software automatically recalculated the reflection spectra to the absorption ones.

The particle micromorphology was observed by SEM using an LEO 1430 device. The Raman spectra were collected in the back-scattering geometry using a triple Raman spectrometer Jobin Yvon T64000 operating in a double subtractive mode. The spectra were recorded with use of a liquid nitrogen-cooled CCD cooled to 140 K . The spectral resolution for the recorded Stokes side Raman spectra was about 1 cm^{-1} (this resolution was achieved by using gratings with $1800\text{ grooves mm}^{-1}$ and $100\text{ }\mu\text{m}$ slits). The deformation of the low-frequency spectral edge by an optical slit, which sometimes smears the right features of low-frequency spectra, was carefully eliminated by rigorous optical alignment. The Raman spectra of BaPrCuS_3 were recorded at the 514.5 nm excitation wavelength from a Spectra Physics Stabilite 2017 laser. To avoid a possible excitation of the Sm^{3+} ion luminescence at the transition to ${}^4\text{F}_{3/2}$ in case of the excitation source specified above, the 647.1 nm line of a Lexel 95 K laser at the 100 mW power (5 mW on the sample) was used as an excitation light source for the Raman spectroscopy of BaSmCuS_3 .

The simultaneous thermal analysis was performed in the He (99.999%, Russia) flow with the use of an STA 449 F3 Jupiter instrument equipped with a (W3%Re – W25%Re) thermocouple. The analyzed powder sample weighed $(90\text{--}100)\pm 0.01\text{ mg}$. The temperature adjustment accuracy was not above 0.3 K . In the temperature range, where thermal events were observed, the heating

rate was 10 K/min . The results of DSK/TG experiments were processed in the Proteus-6 programs package [34]. The possible error in the phase transition enthalpy determination was $\pm 18\%$.

3. Results and discussion

Rietveld refinement was performed using TOPAS 4.2 [35] which accounts the esd's of each point by a special weighting scheme. All peaks measured for BaPrCuS_3 were indexed by an orthorhombic unit cell (space group $Pnma$) with the cell parameters close to those of BaNdCuS_3 [18]. However, the BaSmCuS_3 peaks were indexed by an orthorhombic cell (space group $Cmcm$) with the parameters close to those of KThCuS_3 [36]. Besides, in this sample, a small amount (~5 wt.) of the BaCu_2S_2 (space group $Pnma$) [37] impurity was detected. The crystal structures of BaNdCuS_3 and KThCuS_3 were taken as the starting models for Rietveld refinements.

In order to obtain the model of BaPrCuS_3 , the Nd^{3+} site in BaNdCuS_3 was assumed to be occupied by the Pr^{3+} ion. To obtain the BaSmCuS_3 model, the K^+ site in KThCuS_3 was replaced by Ba, and Th^{4+} was replaced by Sm^{3+} . The thermal parameters of Ba^{2+} , Pr^{3+} and Sm^{3+} ions were refined anisotropically, but Cu^+ and S^{2-} ions were refined with isotropic thermal parameters. The refinements were stable and gave low R -factors (Table 1, Fig. 2). The obtained coordinates, main bond lengths and anisotropic thermal parameters are in Table 2, Tables 1S and 2S, respectively. The crystal structures of BaPrCuS_3 and BaSmCuS_3 are presented in Fig. 3 and they belong to the structure types Eu_2CuS_3 (space group $Pnma$) [29] and KZrCuS_3 (space group $Cmcm$) [30], respectively. The crystallographic data are deposited in Cambridge Crystallographic Data Centre (CSD # 1948871–1948872). The data can be downloaded from the site (www.ccdc.cam.ac.uk/data_request/cif).

Thus, two different structures are observed in BaLnCuS_3 compounds for the sequence Sm-Pm-Nd-Pr. On the one hand, BaSmCuS_3 crystallizes in space group $Cmcm$, and, on the other hand, BaNdCuS_3 and BaPrCuS_3 crystallize in space group $Pnma$. The BaPmCuS_3 structure remains unknown. Accordingly, it is valuable to determine the relation governing the structure type in ABCX_3 crystals. In order to make the space group prediction for the compounds with general formula ABCX_3 , it was decided to consider the structures known for $X = \text{S}, \text{Se}$ from the ICSD database. Generally, the structure consists of AX_7 , BX_7 and CX_4 polyhedra columns parallel to the b -axis, and they join each other by edges, as shown in Fig. S1. The crystal structure deformation and the change of the corresponding space group should depend on ion radii IR(A), IR(B), IR(C) because the column lengths directly depend on them. As it can be reasonably assumed, anion ion radii IR(X) should lead to the overall cell volume deformation without a drastic change of a structure and a space group should not depend on this factor. It is

Table 1
Main parameters of processing and refinement of the BaPrCuS_3 and BaSmCuS_3 samples.

Compound	BaPrCuS_3	BaSmCuS_3
Sp. Gr.	$Pnma$	$Cmcm$
$a, \text{\AA}$	10.56074 (6)	4.07269 (4)
$b, \text{\AA}$	4.11305 (2)	13.4499 (1)
$c, \text{\AA}$	13.42845 (7)	10.3704 (1)
$V, \text{\AA}^3$	583.289 (5)	568.06 (1)
Z	2	2
2θ -interval, $^\circ$	10–150	10–150
$R_{wp}, \%$	1.18	1.84
$R_p, \%$	1.20	1.39
$R_{exp}, \%$	0.62	0.86
χ^2	1.89	2.14
$R_B, \%$	0.79	0.88

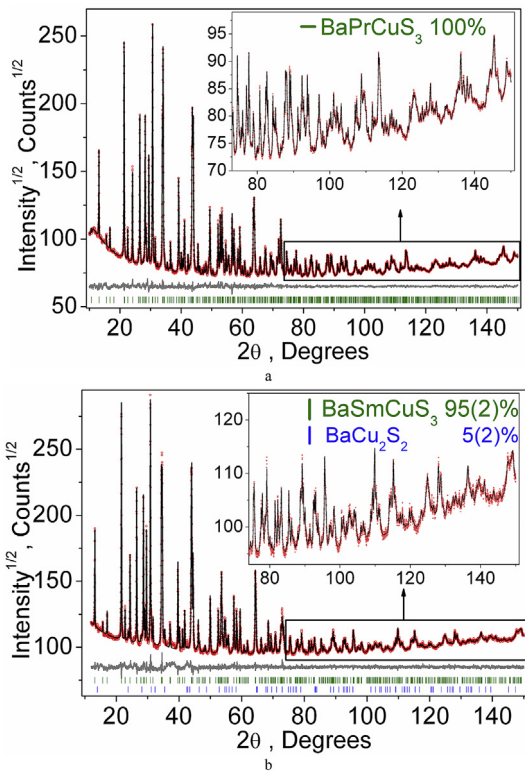


Fig. 2. Difference Rietveld plots of (a) BaPrCuS₃ and (b) BaSmCuS₃.

Table 2

Fractional atomic coordinates and isotropic or equivalent isotropic displacement parameters (\AA^2) of BaPrCuS₃ and BaSmCuS₃.

	x	y	z	$U_{\text{iso}}*/U_{\text{eq}}$
BaPrCuS₃				
Pr	0.00804 (8)	0.25	0.75733 (6)	0.0041 (4)
Cu	0.2406 (2)	0.25	0.28297 (9)	0.0093 (4)*
Ba	0.26735 (8)	0.25	0.00560 (4)	0.0178 (5)
S1	0.0555 (2)	0.25	0.3822 (2)	0.0038 (6)*
S2	0.2558 (3)	0.25	0.6825 (1)	0.0039 (5)*
S3	0.4181 (2)	0.25	0.3905 (2)	0.0070 (7)*
BaSmCuS₃				
Sm	0.5	0	0	0.0090 (4)
Cu	0.5	0.53447 (15)	0.25	0.0128 (8)*
Ba	0.5	0.25634 (7)	0.25	0.0136 (2)
S1	0.5	0.63449 (19)	0.0670 (2)	0.0108 (9)*
S2	0.5	0.9328 (2)	0.25	0.0139 (10)*

valuable to find the tolerance factor $t(\text{IR}(A), \text{IR}(B), \text{IR}(C))$, which controls the space group. But the function is not clear. To solve this problem, a deep learning model with three input neurons $\text{IR}(A)$, $\text{IR}(B)$, $\text{IR}(C)$, two intermediate layers with two neurons and one output neuron was built in package Python 3.6 [38]. The conventional sigmoid activation function was used for all layers. In the model, the output neuron with the 0 value means space group *Pnma*, but 1 means the *Cncm* group. About 2000 epochs of learning were launched and, finally, the small loss function of 5.2% was reached with a high accuracy. The first weight matrix revealed that the weights associated with $\text{IR}(A)$ and $\text{IR}(C)$ neurons are big and positive in the range of 1.3–2. The weights associated with $\text{IR}(B)$ are also big, but negative, and the weight values are in the range from -3.4 to -3.0. Therefore, we can conclude that the tolerance factor should proportionally depend on $\text{IR}(A)$ and $\text{IR}(C)$ values and in the inverse ratio - on $\text{IR}(B)$. Moreover, it was found that the

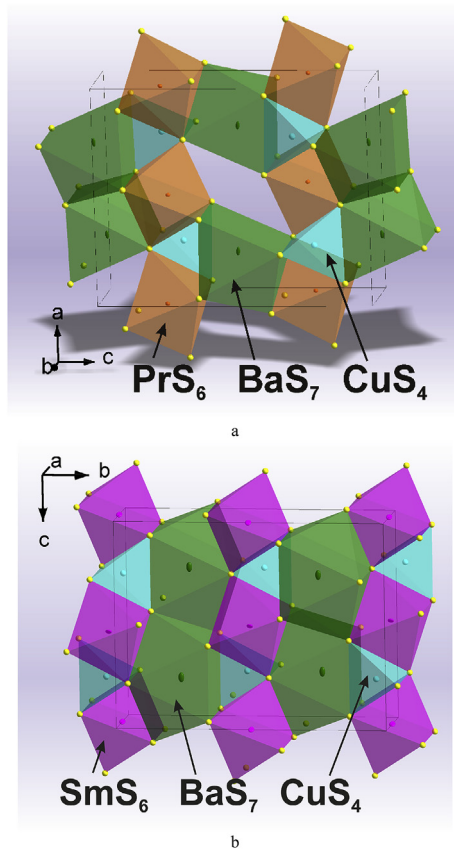


Fig. 3. Crystal structures of (a) BaPrCuS₃ and (b) BaSmCuS₃ sulfides. The anisotropic thermal parameters of Pr³⁺, Sm³⁺ and Ba²⁺ ions are shown at the 50% probability level.

weights corresponding to the $\text{IR}(X)$ neuron are small, and it is in the range of 0.3–0.4. One can really conclude that the output neuron value, i.e. space group, almost does not depend on $\text{IR}(X)$. In addition, as seen in Table 3S [40–54], the pair compounds ABCX₃ with X = S and X = Se are always crystallized in the same space group. Finally, the dimensionless tolerance factor $t = \text{IR}(A) \times \text{IR}(C)/\text{IR}(B)^2$ was suggested. All ABCX₃ (X = S, Se) compounds from ICSD were sorted by increasing the t factor and are presented in Table 3S, and the critical value $t = 0.908$ determines the demarcation line between the *Cmcm* and *Pnma* space groups. As shown in Fig. 4, all ABCX₃ (X = S, Se) compounds can be presented as points in the field determined with two parameters $\text{IR}(A) \times \text{IR}(C)$ and $\text{IR}(B)^2$, and the line $t = \text{IR}(A) \times \text{IR}(C)/\text{IR}(B)^2 = 0.908$ cuts the space into two fields with different space groups. Only two compounds PbYCuS₃ and SrYCuSe₃ (or PbTbCuS₃ and PbDyCuS₃) positioned in the vicinity to the demarcation line and the related points are away from the general trend. First, the structures of these compounds should be investigated more carefully. As for the prediction of the structure type for BaPmCuS₃, it seems to be impossible because the related point is assumed to appear on the demarcation line.

The thermal, morphological and spectroscopic properties were measured only for phase-pure BaPrCuS₃. As it was shown by the XRD analysis, the available BaSmCuS₃ sample contains a significant impurity of BaCu₂S₂. Several attempts were made in the synthesis of phase-pure BaSmCuS₃ by the sulphidation technique with some variation of the technological parameters. However, in all experiments, the presence of BaCu₂S₂ was observed in the final products. The source of this effect is presently unknown, and, accordingly, the synthesis conditions should be optimized to get the phase-pure BaSmCuS₃ product.

Table 3

Temperature of melting and enthalpy of melting in compounds ABCuS_3 .

Compound	T_{melt} , K	H_{melt} , $\text{kJ} \cdot \text{mol}^{-1}$	Reference
SrLaCuS_3	1513	6,9	[24,25]
SrCeCuS_3	1468	5,2	[25,46]
SrPrCuS_3	1459	13,2	[25]
SrNdCuS_3	1429	16,8	[25]
SrSmCuS_3	1605	2,8	[25]
EuLaCuS_3	1539	23,4	[32,56]
EuCeCuS_3	1524	23,7	[55]
EuPrCuS_3	1497	20,1	[55]
EuNdCuS_3	1470	17,7	[39,55]
EuDyCuS_3	1727	2,9	[28]
BaGdCuS_3	1685	—	[39]
BaPrCuS_3	1580.9	86.6	This study

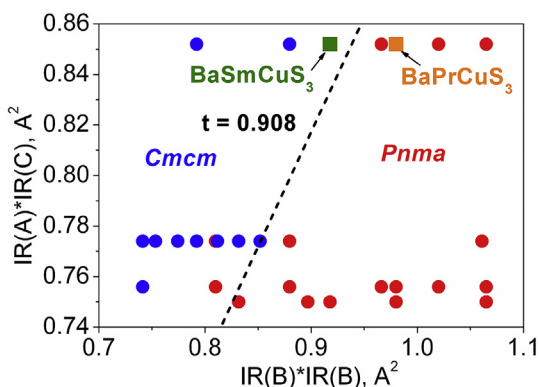


Fig. 4. Structure types in the known ABCX_3 ($\text{X} = \text{S}, \text{Se}$) crystals.

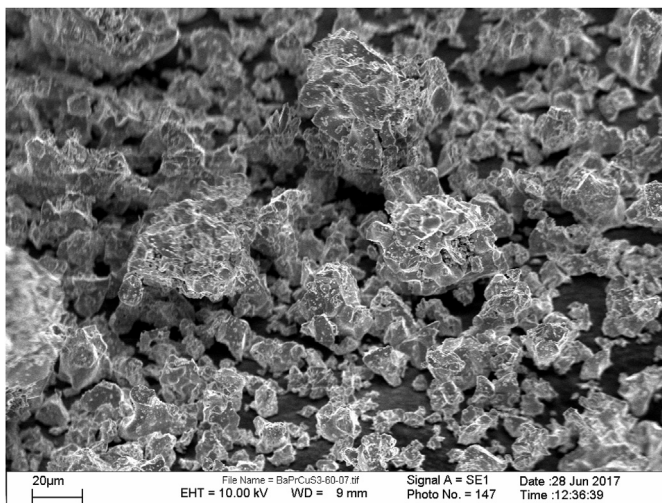


Fig. 5. SEM image of BaPrCuS_3 powder.

The BaPrCuS_3 powder micromorphology is shown in Fig. 5. The powder contains irregular partly agglomerated particles sized $\sim 1\text{--}5 \mu\text{m}$. The faceted shapes were not detected and this may be a result of a drastic anion exchange during the sulfidation reaction at high temperatures. Under the conditions, the formation of faceted microcrystal shapes seems to be highly improbable. The thermal properties of BaPrCuS_3 powder were analyzed over the temperature range from 300 to 1800 K and the related curves are shown in Fig. 6. The sample weight was 102.8 mg and the weight loss was not registered in the temperature cycling. The

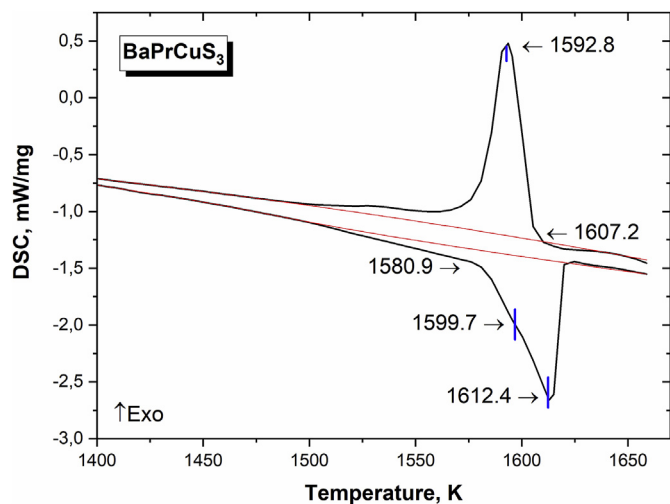


Fig. 6. DTA curves recorded for BaPrCuS_3 . The baselines are shown in red color. (For interpretation of the references to color in this figure legend, the reader is referred to the Web version of this article.)

endothermic effect related to the substance melting was observed at $T_{\text{melt}} = 1580.9$ K upon heating, and the exothermic effect due to the substance crystallization was detected at $T_{\text{cryst}} = 1607.2$ K. Thus, the effect of overcooling is expressed for BaPrCuS_3 and the difference between melting and crystallization points is 27 K. The effect of overcooling is bound to the incongruent type of melting. On the heating curve, the melting peak splitting into two components at 1599 K and 1612 K is evident. The heat of melting determined for BaPrCuS_3 is equal to $\Delta H_{\text{melt}} = 86.6 \text{ kJ mol}^{-1}$.

At present, the thermal characteristics of ALnCuS_3 compounds are less studied. The thermal parameters available in the literature are summarized in Table 3 [55]. It should be noted that nearly all observed ALnCuS_3 compounds melt incongruently. As seen, the melting temperature values obtained for SrLnCuS_3 and EuLnCuS_3 sulfides are similar for the same Ln element. It is particularly interesting to compare the melting temperatures of the APrCuS_3 ($\text{A} = \text{Sr, Eu, Ba}$) set. The melting temperature of BaPrCuS_3 is noticeably higher than that of APrCuS_3 ($\text{A} = \text{Sr, Eu}$) and, presumably, this relation indicates a higher thermal stability of the sulfides with a bigger A element radius. The effect of lanthanide compression can also increase the thermal stability of ALnCuS_3 compounds. Indeed, BaGdCuS_3 melts congruently at as high temperature as 1685 K [22] and the temperature is significantly higher than that of BaPrCuS_3 . The heat of melting obtained for BaPrCuS_3 is also noticeably higher than that of APrCuS_3 ($\text{A} = \text{Sr, Eu}$) and it is similar to the values known for simple sulfides Ln_2S_3 [56].

To the best of our knowledge, the calculations of the band structures of BaPrCuS_3 and BaSmCuS_3 are absent in the literature. However, in this situation, the available band structure calculations for monoclinic sulfides $\text{Ba}_2\text{Cu}_2\text{ThS}_5$ and $\text{Ba}_2\text{Cu}_2\text{US}_5$ (space group $C2/m$) [57] can be used for the initial observation of the BaPrCuS_3 band structure. Thus, it is reasonably assumed that the valence band top in BaPrCuS_3 could be formed by $\text{S} 2p$, $\text{Cu} 3d$ and $\text{Pr} 4f$ orbitals, while the conduction band bottom is formed by the contributions from all ions, including 5 d orbitals of Ba and Pr. The strong band energy dependence on the direction in Brillouin zone is expected and, therefore, both direct and indirect allowed transitions can contribute to the fundamental absorption edge formation.

The Tauc plot, in the case of indirect allowed transitions, for the UV-visible spectra recorded for BaPrCuS_3 , is shown in the insert of Fig. 7. The optical bandgap estimated for BaPrCuS_3 is equal to 2.1 eV. This value is close to the bandgap value 2.00 eV earlier determined

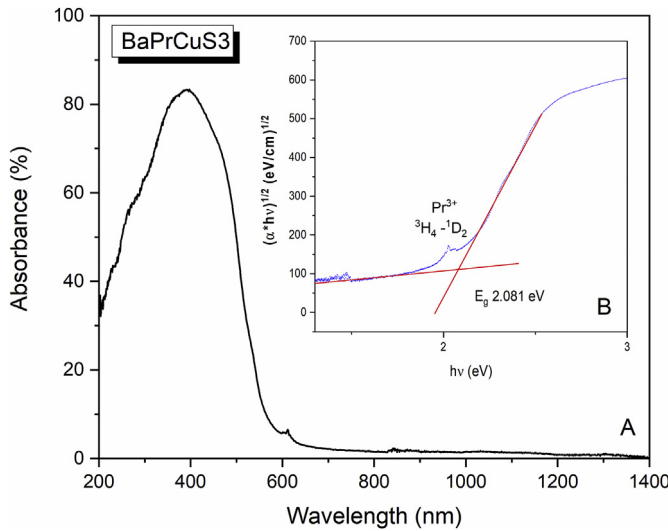


Fig. 7. Absorption spectrum for BaPrCuS₃. Inset: Tauc plot for BaPrCuS₃.

for BaLaCuS₃ [17], as well as to the bandgap of another recently studied sulfide EuErCuS₃ (1.94 eV) [68]. At the same time, the imperfect linearity of experimental spectrum in the region up to 2.5 eV indicates the contribution of other transition types in accordance with the previously formulated assumption. Besides the fundamental absorption band, the minor narrow peak at ~2 eV can be detected in the spectrum and it is ascribed to the *f-f* transition of Pr³⁺ ions, namely, $^3H_4 - ^1D_2$. Other prominent *f-f* transitions of the Pr³⁺ ion, namely, $^3H_4 - ^3P_J$ ($J = 0, 1, 2$) and 1S_0 , cannot be resolved in the obtained spectrum, and, therefore, it should be deduced that the 3P_J levels of Pr³⁺ are immersed into the BaPrCuS₃ conduction band. At the same time, the *f-d* transition of Pr³⁺ ions should be supposed as contributing to the fundamental absorption band formation.

The emission spectrum obtained from BaPrCuS₃ under the excitation at 514.5 nm is shown in Fig. S2. The left part of this spectrum in the range below 525 nm is formed by the Raman spectrum with its narrow lines. At the wavelengths above 525 nm, the broad band peaking at 650 nm is observed. This spectral band must be assigned to the luminescence from the conduction band of the electronic structure of BaPrCuS₃. The contribution from the Pr³⁺ ion *f-f* transitions to the luminescence is obviously absent since the 514.5 nm excitation is inefficient to excite the energy level system of *f* electrons in the Pr³⁺ ion. The luminescence intensity is comparable to that of Raman spectrum. Therefore, BaPrCuS₃ is highly likely to be an indirect wide-bandgap semiconductor, in accordance with the assumption stated above. The energy spacing of the spectral replicas observed in the luminescent band is equal to 0.05 eV (400 cm⁻¹). The corresponding vibrational frequencies are absent in the crystal structure of BaPrCuS₃. Therefore, the origin of these replicas cannot be ascribed to the well-known phonon replicas in the exciton luminescence and needs a special investigation.

The Raman spectra from BaPrCuS₃ and BaSmCuS₃ powders are given in Fig. 8. For BaPrCuS₃, belonging to space group *Pnma*, the mechanical representation at the Brillouin zone (BZ) center can be written as

$$\Gamma_{\text{vibr}} = 12A_g + 6A_u + 6B_{1g} + 12B_{1u} + 12B_{2g} + 6B_{2u} + 6B_{3g} + 12B_{3u},$$

where the Raman active modes are

$$\Gamma_{\text{Raman}} = 12A_g + 6B_{1g} + 12B_{2g} + 6B_{3g} [59].$$

The vibrational irreducible representation at the Γ point of BZ for BaSmCuS₃ is $\Gamma_{\text{vibr}} = 5A_g + 2A_u + 4B_{1g} + 7B_{1u} + B_{2g} + 7B_{2u} + 5B_{3g} + 5B_{3u}$, where Raman active modes are $\Gamma_{\text{Raman}} = 5A_g + 4B_{1g} + B_{2g} + 5B_{3g}$. The difference between

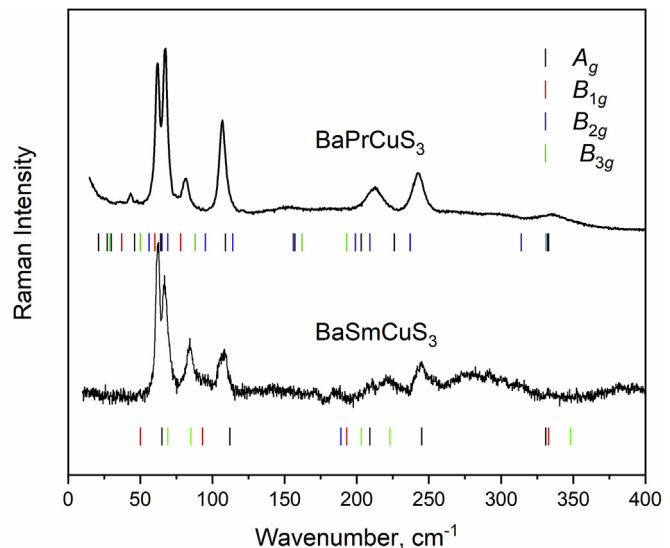


Fig. 8. Raman spectra of BaPrCuS₃ and BaSmCuS₃. The black, red, blue and green vertical ticks mark the calculated wavenumbers of Raman-active vibrational modes. (For interpretation of the references to color in this figure legend, the reader is referred to the Web version of this article.)

the Cu–S1 (Cu–S3) bond lengths in BaPrCuS₃ and Cu–S1 in BaSmCuS₃ is equal to 0.04 Å; it is equal to 0.007 Å between Cu–S2 bond lengths in BaPrCuS₃ and Cu–S2 in BaSmCuS₃. Thus, the spectral band positions, related to the vibrational modes of CuS₄ tetrahedra, should not differ significantly, but the number of spectral bands should not be the same. The set of Raman spectra in several scattering geometries should be obtained to get the bands related to specified Raman modes. However, in the case of powder samples, such measurements are impossible.

In order to interpret the observed Raman spectra, the calculation of BaPrCuS₃ and BaSmCuS₃ lattice dynamics using the program package LADY [60] was performed. The atomic vibration values were obtained using the simplified version of Born-Karman model [61]. Within this model, only the pair-wise interactions and bond-stretching force constants *F* are considered and the model implies that *F* depends on r_{ij} (interatomic distance). The $F(r_{ij})$ dependences are the same for all atom pairs: $F(r_{ij}) = \lambda \exp(-r_{ij}/\rho)$, where λ and ρ are the parameters characterizing a selected pair interaction. To find the model parameters, a special optimization program was written and tested for several representative compounds [62–68].

As it was noted above, BaPrCuS₃ and BaSmCuS₃ are members of the ALnCuS₃ sulfide family and their structures are formed by the layers of CuS₄ tetrahedra and LnS₆ octahedra [29,30]. According to the lattice dynamics simulations, vibrations at low wavenumbers (20–115 cm⁻¹) are related to the vibration of such layers. For example, the lowest wavenumber Raman-active mode in BaPrCuS₃ is graphically shown in Fig. 9(a). The strong bands at 62 and 67 cm⁻¹ in BaPrCuS₃ and BaSmCuS₃ are related to the antisymmetric displacements of structural layers, and the vibrations are shown in Fig. 9(b) and (c), respectively. The difference between BaPrCuS₃ and BaSmCuS₃ in Raman spectra should be in the range of 115–185 cm⁻¹. There are no traces of Raman-active vibrational modes in this range in the case of BaSmCuS₃, but a group of lines is observed in the case of BaPrCuS₃ (Fig. 8). The region of Raman spectra between 188 and 250 cm⁻¹ is related to the vibrations of sulfur ions mainly and, for example, the bending vibration of CuS₄ in BaSmCuS₃ is shown in Fig. 9(d). It is clearly seen in Fig. S1 that the CuS₄ tetrahedra from the neighboring unit cells share one common vertex and the related vibration of bridged sulfur ion appears in the

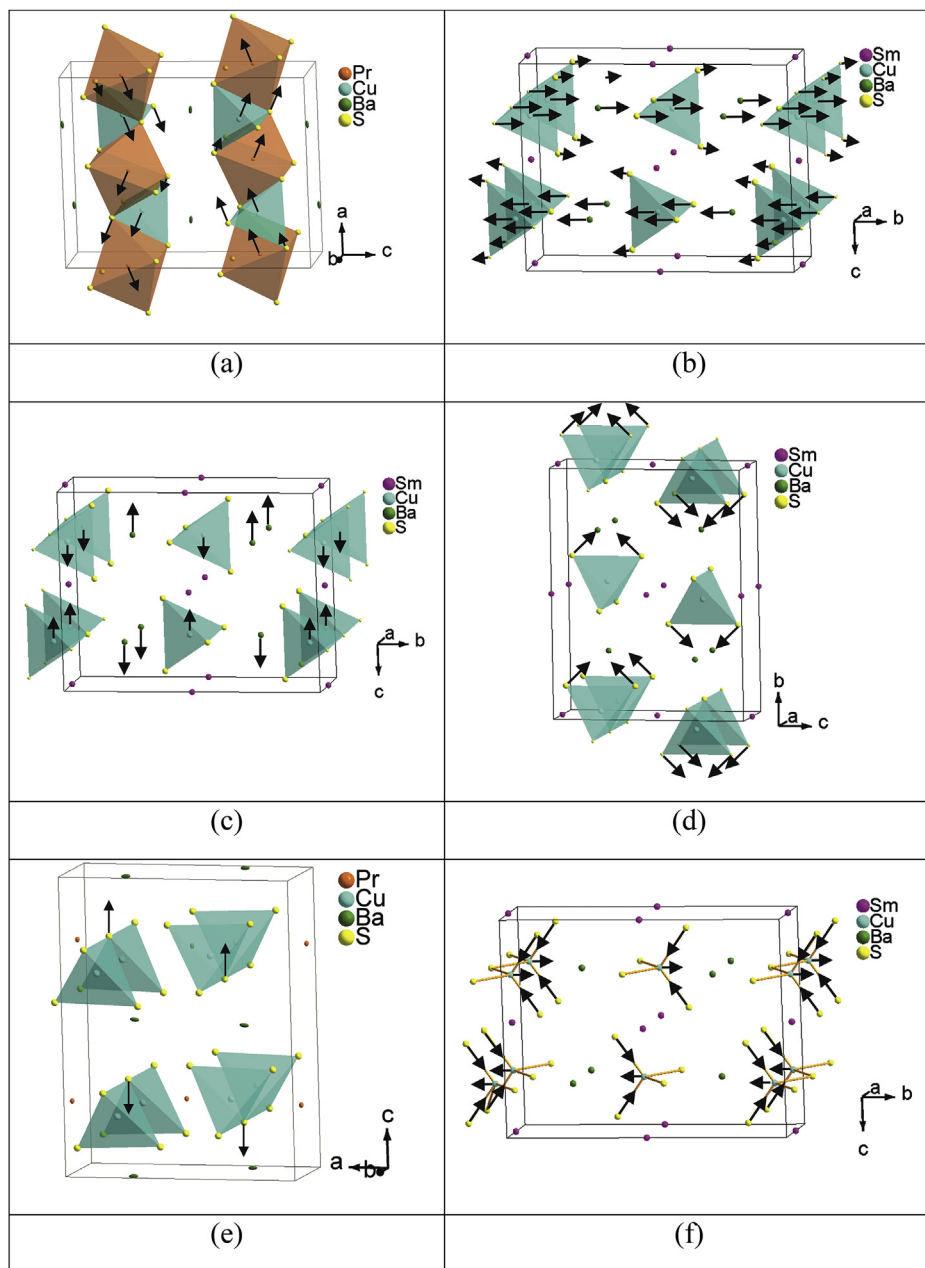


Fig. 9. Examples of calculated vibrational modes in BaPrCuS_3 , (a) A_g 20.6 cm^{-1} low frequency layer vibration, (e) A_g 202.5 cm^{-1} related to the vibration of bridging oxygen atoms and in BaSmCuS_3 , (b) and (c) A_g 64.6 cm^{-1} and B_{3g} 68.6 cm^{-1} layer vibrations, respectively, (d) A_g 209.2 cm^{-1} O–S–O bending-like vibration, (f) A_g 330.6 cm^{-1} S–O stretching-like vibration.

spectra as a spectral band of around 242 cm^{-1} (Fig. 9(e)). The stretching-like vibrations in CuS_4 tetrahedra are in the high wavenumber range of $310\text{--}350 \text{ cm}^{-1}$, and they are shown in Fig. 9(f).

4. Conclusion

This study addresses the synthesis, structure, optical and thermal properties of the new complex sulfides BaPrCuS_3 (space group $Pnma$) and BaSmCuS_3 (space group $Cmcm$). The compounds crystallize in two different orthorhombic structures that open a possibility to analyze the structure transformation mechanism in the known $ABCX_3$ ($X = \text{S}, \text{Se}$) compounds for the sequence Sm-Pm-Nd-Pr . To solve this problem, the deep learning neuron model was built

on the base of the known $ABCX_3$ compounds. The introduced tolerance factor $t = \text{IR}(A) \times \text{IR}(C)/\text{IR}(B)^2$ can be used as a robust indicator for the prediction of the structure type for compounds $ABCX_3$ ($X = \text{S}, \text{Se}$) which crystal structure remains unknown. BaPrCuS_3 is shown to be the indirect bandgap compound with bandgap width 2.1 eV .

Author contribution

Nikita O. Azarapin: sample synthesis, thermal measurements, paper writing. Aleksandr S. Aleksandrovsky: spectroscopic analysis, paper writing. Victor V. Atuchin: conceptualization, paper writing, corresponding author. Tatyana A. Gavrilova: SEM measurements and interpretation. Aleksandr S. Krylov: Raman measurements and

interpretation. Maxim S. Molokeev: structural measurements and interpretation, paper writing. Shaibal Mukherjee: conceptualization, paper writing. Aleksandr S. Oreshonkov: Raman spectra interpretation and paper writing. Oleg V. Andreev: conceptualization, paper writing.

Declaration of competing interests

The authors declare that they have no known competing financial interests or personal relationships that could have appeared to influence the work reported in this paper.

The authors declare the following financial interests/personal relationships which may be considered as potential competing interests: We have no known competing financial interests or personal relationships that could have appeared to influence the work reported in this paper.

We have no known competing financial interests or personal relationships that could have appeared to influence the work reported in this paper.

Acknowledgements

This study was supported by the Russian Science Foundation (19-42-02003). Also, this study was supported by RFBR (18-32-20011, 18-03-00750, in part of Raman analysis). This work was partially supported by DST-RSF project under the India-Russia Programme of Cooperation in Science and Technology (No. DST/INT/RUS/RSF/P-20 dated May 16, 2019). Shaibal Mukherjee would like to thank the Ministry of Electronics and Information Technology (MeitY) for the Young Faculty Research Fellowship (YFRF) under Visvesvaraya Ph.D. Scheme for Electronics and IT. This publication is an outcome of the R&D work undertaken in the project under the Visvesvaraya Ph.D. Scheme of MeitY being implemented by Digital India Corporation (formerly Media Lab Asia). SEM investigations were carried out using the equipment of CKP "Nanostructures", Novosibirsk, Russia.

Appendix A. Supplementary data

Supplementary data to this article can be found online at <https://doi.org/10.1016/j.jallcom.2019.153134>.

References

- [1] L.A. Koscielski, J.A. Ibers, The structural chemistry of quaternary chalcogenides of the type $AMM'Q_3$, *Z. Anorg. Allg. Chem.* 638 (15) (2012) 2585–2593.
- [2] C. Coughlan, M. Ibáñez, O. Dobrozhany, A. Singh, A. Cabot, K.M. Ryan, Compound copper chalcogenide nanocrystals, *Chem. Rev.* 117 (9) (2017) 5865–6109.
- [3] W.L. Yin, K. Feng, R. He, D.J. Mei, Z.S. Lin, J.Y. Yao, Y.C. Wu, $BaGa_2MQ_6$ ($M = Si, Ge; Q = S, Se$): a new series of promising IR nonlinear optical materials, *Dalton Trans.* 41 (2012) 5653–5661.
- [4] A.P. Yelisseyev, M.K. Starikova, V.V. Korolev, L.I. Isaenko, S.I. Lobanov, Photoluminescence of lithium thiogallate $LiGaS_2$, *J. Am. Opt. Soc. B* 29 (5) (2012) 1003–1011.
- [5] A.H. Reshak, I.V. Kityk, O.V. Parasyuk, H. Kamarudin, S. Auluck, Influence of replacing Si by Ge in the chalcogenide quaternary sulfides $Ag_2In_2Si(Ge)S_6$ on the chemical bonding, linear and nonlinear optical susceptibilities, and hyperpolarizability, *J. Phys. Chem. B* 117 (8) (2013) 2545–2553.
- [6] V.V. Atuchin, S.V. Borisov, S.A. Magarill, N.V. Pervukhina, Sphalerite framework in polar sulfides, *J. Chem. Crystallogr.* 43 (9) (2013), 488–192.
- [7] Yu.A. Murashko, A.V. Ruseikina, A.A. Kislytsyn, O.V. Andreev, Optical and thermal properties of the $EuLnCuS_3$ ($Ln = La, Pr, Sm, Gd$) compounds, *Inorg. Mater.* 51 (12) (2015) 1213–1218.
- [8] D.J. Mei, S.Y. Zhang, F. Liang, S.G. Zhao, J.Q. Jiang, J.B. Zhong, Z.S. Lin, Y.D. Wu, $LiGaGe_2S_6$: a chalcogenide with good infrared nonlinear optical performance and low melting point, *Inorg. Chem.* 56 (21) (2017) 13267–13273.
- [9] A.A. Ionin, D.V. Badikov, V.V. Badikov, I.O. Kinyaevskiy, Yu.M. Klimachev, A.A. Kotkov, A.Yu. Kozlov, A.M. Sagitova, D.V. Sinitsyn, Sum frequency generation of multi-line slab radio frequency discharge carbon monoxide laser system with intracavity nonlinear $BaGa_2GeSe_6$ crystal, *Opt. Lett.* 43 (18) (2018) 4358–4361.
- [10] A.O. Fedorchuk, O.V. Parasyuk, O. Cherniushok, B. Andriyevsky, G.L. Myronchuk, O.Y. Khuzhun, G. Lakshminarayana, J. Jedryka, I.V. Kityk, A.M. ElNaggar, A.A. Albassam, M. Piasecki, $PbGa_2GeS_6$ crystal as a novel nonlinear optical material: band structure aspects, *J. Alloy. Comp.* 740 (2018) 294–304.
- [11] W.-J. Yin, Y.L. Wu, S.-H. Wei, R. Noufi, M.M. Al-Jassim, Y.F. Yan, Engineering grain boundaries in $Cu_2ZnSnSe_4$ for better cell performance: a first-principle study, *Adv. Energy Mater.* 4 (2014) 1–5.
- [12] V. Awasthi, S.K. Pandey, S.K. Pandey, S. Verma, M. Gupta, S. Mukherjee, Growth and characterizations of dual ion beam sputtered CLGS thin films for photovoltaic applications, *J. Mater. Sci. Mater. Electron.* 25 (7) (2014) 3069–3076.
- [13] M. Nguyen, K. Ernits, K.F. Tai, C.F. Ng, S.S. Pramana, W.A. Sasangka, S.K. Batabyal, T. Holopainen, D. Meissner, A. Neisser, L.H. Wong, ZnS buffer layer for $Cu_2ZnSn(SSe)_4$ monograins layer solar cell, *Sol. Energy* 111 (2015) 344–349.
- [14] K.-J. Yang, D.-H. Son, S.-J. Sung, J.-H. Sim, Y.-I. Kim, S.-N. Park, D.-H. Jeon, J.S. Kim, D.-K. Hwang, C.-W. Jeon, D.H. Nam, H.S. Cheong, J.-K. Kang, D.-H. Kim, A band-gap-graded CZTSSe solar cell with 12.3% efficiency, *J. Mater. Chem. A* 4 (2016) 10151–10158.
- [15] B.S. Sengara, V. Garg, A. Kumar, V. Awasthi, S. Kumar, V.V. Atuchin, S. Mukherjee, Band alignment of Cd-free $(Zn, Mg)O$ layer with $Cu_2ZnSn(SSe)_4$ and its effect on the photovoltaic properties, *Opt. Mater.* 84 (2018) 748–756.
- [16] V. Garg, B.S. Sengar, V. Awasthi, A. Kumar, R. Singh, S. Kumar, C. Mukherjee, V.V. Atuchin, S. Mukherjee, Investigation of dual-ion beam sputter-instigated plasmon generation in TCOs: a case study of GZO, *ACS Appl. Mater. Interfaces* 10 (2018) 5464–5474.
- [17] A.E. Christuk, P. Wu, J.A. Ibers, New quaternary chalcogenides $BaLnMQ_3$ ($Ln =$ rare earth; $M = Cu, Ag; Q = S, Se$. I. Structures and grinding-induced phase transition in $BaLaCuQ_3$), *J. Solid State Chem.* 110 (1994) 330–336.
- [18] P. Wu, A.E. Christuk, J.A. Ibers, New quaternary chalcogenides $BaLnMQ_3$ ($Ln =$ rare earth or Sc; $M = Cu, Ag; Q = S, Se$. II. Structures and property variation vs rare-earth element), *J. Solid State Chem.* 110 (1994) 337–344.
- [19] Y. Yang, J.A. Ibers, Synthesis and characterization of a series of quaternary chalcogenides $BaLnMQ_3$ ($Ln =$ rare earth, $M =$ coinage metal, $Q = Se$ or Te), *J. Solid State Chem.* 147 (1999) 366–371.
- [20] F.Q. Huang, K. Mitchell, J.A. Ibers, New layered materials: syntheses, structures, and optical and magnetic properties of $CsGdZnSe_3$, $CsZrCuSe_3$, $CsU-CuSe_3$, and $BaGdCuSe_3$, *Inorg. Chem.* 40 (2001) 5123–5126.
- [21] K. Mitchell, F.Q. Huang, A.D. McFarland, C.L. Haynes, R.C. Somers, R.P. Van Duyne, J.A. Ibers, The $CsLnMS_3$ semiconductors ($Ln =$ rare-earth element; $Y; M = Zn, Cd, Hg$), *Inorg. Chem.* 42 (2003) 4109–4116.
- [22] N.V. Sikerina, A.V. Solov'yev, E.N. Toroshchin, O.V. Andreev, Phase equilibria in the $Ba-S-Cu_2S-Gd_2S_3$ system, *Russ. J. Inorg. Chem.* 52 (12) (2007) 1982–1986.
- [23] N.V. Sikerina, O.V. Andreev, I.P. Leven, Interactions in the $SrS-Cu_2S-Ln_2S_3$ ($Ln = Gd$ or Er) systems and phase-formation laws in the $SrS-Cu_2S-Ln_2S_3$ ($Ln = La-Lu$) systems, *Russ. J. Inorg. Chem.* 53 (3) (2008) 455–459.
- [24] A.V. Ruseikina, L.A. Solov'yev, O.V. Andreev, Crystal structures and properties of $SrLnCuS_3$ ($Ln = La, Pr$), *Russ. J. Inorg. Chem.* 59 (3) (2014) 196–201.
- [25] A.V. Ruseikina, O.V. Andreev, E.O. Galenko, S.I. Kol'tsov, Trends in thermodynamic parameters of phase transitions of lanthanide sulfides $SrLnCuS_3$ ($Ln = La-Lu$), *J. Therm. Anal. Calorim.* 128 (2) (2017) 993–999.
- [26] A.V. Ruseikina, O.V. Andreev, Regularities of change in the structural parameters of $EuLnCuS_3$ ($Ln = La-Nd, Sm, Gd, Ho$), *Russ. J. Inorg. Chem.* 62 (2) (2017) 160–167.
- [27] A.V. Ruseikina, S.I. Kol'tsov, O.V. Andreev, L.A. Pimneva, Crystal structure of $EuLnAgS_3$ ($Ln = Gd$ and Ho) compounds, *Russ. J. Inorg. Chem.* 62 (12) (2017) 1632–1637.
- [28] A.V. Ruseikina, O.V. Andreev, Phase equilibria in systems $DyCuS_2-Eu-S$ and $Cu_2S-Dy_2S_3-Eu-S$, *Russ. J. Inorg. Chem.* 63 (11) (2018) 1494–1500.
- [29] P. Lemoine, D. Carre, M. Guittard, Structure du sulfure d'europtium et de cuivre Eu_2CuS_3 , *Acta Crystallogr. C* 42 (1986) 390–391.
- [30] M.F. Mansuetto, P.M. Keane, J.A. Ibers, Synthesis, structure, and conductivity of the new group IV chalcogenides $KCuZrQ_3$ ($Q = S, Se, Te$), *J. Solid State Chem.* 101 (1992) 257–264.
- [31] N.A. Khrithin, O.V. Andreev, O.V. Mitroshin, A.S. Korotkov, Thermodynamics of phase changes in systems $BaS-Ln_2S_3$ ($Ln = Pr, Sm, Gd, Tb, Er, Lu$), *J. Phase Equilibria Diffusion* 25 (6) (2004) 515–519.
- [32] A.V. Ruseikina, O.V. Andreev, Phase equilibria in the $Cu_2S-La_2S_3-EuS$ system, *Russ. J. Inorg. Chem.* 62 (5) (2017) 610–618.
- [33] M. Ohta, S. Hirai, H. Kato, V.V. Sokolov, V.V. Bakovets, Thermal decomposition of NH_4SCN for preparation of Ln_2S_3 ($Ln = La$ and Gd) by sulfurization, *Mater. Trans.* 50 (7) (2009) 1885–1889.
- [34] NETZSCH Proteus 6, Thermic Analyses – User's and Software Manuals, 2012, Germany.
- [35] Bruker AXS TOPAS V4, General Profile and Structure Analysis Software for Powder Diffraction Data. – User's Manual, Bruker AXS, Karlsruhe, Germany, 2008.
- [36] H.D. Selby, B.C. Chan, R.F. Hess, K.D. Abney, P.K. Dorhout, Three new phases in the $K/Cu/Th/S$ system: $KCuThS_3$, $K_2Cu_2ThS_4$, and $K_3Cu_3Th_2S_7$, *Inorg. Chem.* 44 (18) (2005) 6463–6469.
- [37] J. Huster, W. Bronger, α - und β - $BaCu_2X_2$ ($X \triangleq S, Se$) – darstellung von Einkristallen in Kaliumchalcogenocyanat-Schmelzen, *Z. Anorg. Allg. Chem.* 625 (12) (1999) 2033–2040.

- [38] <https://www.python.org/>.
- [39] A.V. Ruseikina, L.A. Solovyev, O.V. Andreev, A.A. Kislytsyn, EuNdCuS₃: crystal structure of the high-temperature polymorph and properties, Russ. J. Inorg. Chem. 59 (10) (2014) 1109–1114.
- [40] M.A. Eberle, S. Strobel, T. Schleid, SrCuNdS₃: a new compound with two different crystal structures. Jahrestagung der DGK, Berlin, 17–20 Maerz 2014, 2014, 1 MS05-48, MS05-48 DUMMY7.
- [41] I. Kohatsu, B.J. Wuensch, The crystal structure of aikinite, PbCuBiS₃, Acta Crystallogr. B 27 (6) (1971) 1245–1252.
- [42] S. Strobel, T. Schleid, Three structure types for strontium copper (I) lanthanide (III) selenides SrCuMSe₃ (M= La, Gd, Lu), J. Alloy. Comp. 418 (1–2) (2006) 80–85.
- [43] A.V. Ruseikina, L.A. Solov'ev, O.V. Andreev, Crystal structures of α -and β -EuPrCuS₃, Russ. J. Inorg. Chem. 58 (10) (2013) 1231–1236.
- [44] N.V. Sikerina, O.V. Andreev, Crystal structures of SrLnCuS₃ (Ln=Gd, Lu), Russ. J. Inorg. Chem. 52 (4) (2007) 581–584.
- [45] S. Strobel, T. Schleid, Quaternäre Strontium-Kupfer (I)-Lanthanoid (III)-Selenide mit Cer und Praseodym: SrCuCeSe₃ und SrCuPrSe₃, ein ungleiches Geschwisterpaar/Quaternary Strontium Copper (I) Lanthanoid (III) Selenides with Cerium and Praseodymium: SrCuCeSe₃ and SrCuPrSe₃, Unequal Brother and Sister, Z. Naturforschung B 59 (9) (2004) 985–991.
- [46] A.V. Ruseikina, L.A. Solov'ev, Crystal structures of α - and β -SrCeCuS₃, Russ. J. Inorg. Chem. 61 (4) (2016) 482–487.
- [47] A.V. Ruseikina, L.A. Solovyov, M.S. Molokeev, O.V. Andreev, Crystal structures of EuLnCuS₃ (Ln= Nd and Sm), Russ. J. Inorg. Chem. 57 (1) (2012) 79–83.
- [48] F. Furuchi, M. Wakushima, Y. Hinatsu, Magnetic properties and ¹⁵¹Eu Mössbauer effects of mixed valence europium copper sulfide, Eu₂CuS₃, J. Solid State Chem. 177 (11) (2004) 3853–3858.
- [49] L.D. Gulay, I.D. Olekseyuk, Crystal structures of the RCuPbSe₃ (R=Gd, Tb, Dy, Ho, Er, Tm, Yb and Lu) compounds, J. Alloy. Comp. 387 (1–2) (2005) 160–164.
- [50] M. Wakushima, F. Furuchi, Y. Hinatsu, Crystal structures and magnetic properties of novel rare-earth copper sulfides, EuRCuS₃ (R=Y, Gd–Lu), J. Phys. Condens. Matter 16 (30) (2004) 5503.
- [51] L.D. Gulay, M.R. Huch, I.D. Olekseyuk, J. Stepień-Damm, A. Pietraszko, Crystal structures of the compounds Yb_{5.5}AgSe₈, YbAgSe₂ and Y_xYb_{1-x}CuYbSe₃ (x=0.11), J. Alloy. Comp. 428 (1–2) (2007) 139–145.
- [52] S. Maier, J. Prakash, D. Berthebaud, O. Perez, S. Bobev, F. Gascoin, Crystal structures of the four new quaternary copper (I)-selenides A_{0.5}CuZrSe₃ and ACuYSe₃ (A=Sr, Ba), J. Solid State Chem. 242 (2016) 14–20.
- [53] L.D. Gulay, V.Y. Shemet, I.D. Olekseyuk, Crystal structures of the compounds YCuS₂, Y₃CuSnS₇ and YCuPbS₃, J. Alloy. Comp. 388 (1) (2005) 59–64.
- [54] F.Q. Huang, J.A. Ibers, New layered materials: syntheses, structures, and optical properties of K₂TiCu₂S₄, Rb₂TiCu₂S₄, Rb₂TiAg₂S₄, Cs₂TiAg₂S₄, and Cs₂Ti-Cu₂Se₄, Inorg. Chem. 40 (11) (2001) 2602–2607.
- [55] A.V. Ruseikina, A.V. Kertman, Synthesis of Compounds EuLnCuS₃ (Ln=La-Nd), Temperature and Enthalpy of Melting, vol. 3, Vestnik of the Tumen State University, 2010, pp. 221–227 (in Russian).
- [56] P.O. Andreev, A.A. Polkovnikov, Y.G. Denisenko, O.V. Andreev, T.M. Burhanova, A.N. Bobylev, L.A. Pimneva, Temperatures and enthalpies of melting of Ln₂S₃ (Ln=Gd, Tb, Dy, Ho, Er, Tm, Yb, and Lu) compounds, J. Therm. Anal. Calorim. 131 (2) (2018) 1545–1551.
- [57] A. Mesbah, S. Lebegue, J.M. Klingsporn, W. Stojko, R.P. Van Duyne, J.A. Ibers, Synthesis, crystal structure, and optical properties of Ba₂Cu₂ThS₅, and electronic structures of Ba₂Cu₂ThS₅ and Ba₂Cu₂US₅, J. Solid State Chem. 200 (2013) 349–353.
- [58] E. Kroumova, M.I. Aroyo, J.M. Perez-Mato, A. Kirov, C. Capillas, S. Ivantchev, H. Wondratschek, Bilbao Crystallographic Server: useful databases and tools for phase-transition studies, Phase Transitions 76 (2003) 155–170.
- [59] M.B. Smirnov, V.Yu Kazimirov, LADY: Software for Lattice Dynamics Simulations, JINR communications, 2001, E 14–2001–159.
- [60] M. Smirnov, R. Baddour-Hadjean, Li intercalation in TiO₂ anatase: Raman spectroscopy and lattice dynamic studies, J. Chem. Phys. 121 (2004) 2348–2355.
- [61] Yu.G. Denisenko, V.V. Atuchin, M.S. Molokeev, A.S. Aleksandrovsky, A.S. Krylov, A.S. Oreshonkov, S.S. Volkova, O.V. Andreev, Structure, thermal stability, and spectroscopic properties of triclinic double sulfate AgEu(SO₄)₂ with isolated SO₄ groups, Inorg. Chem. 57 (2018) 13279–13288.
- [62] V.V. Atuchin, A.S. Aleksandrovsky, M.S. Molokeev, A.S. Krylov, A.S. Oreshonkov, D. Zhou, Structural and spectroscopic properties of self-activated monoclinic molybdate BaSm₂(MoO₄)₄, J. Alloy. Compd. 729 (2017) 843–849.
- [63] C.S. Lim, Aleksandr S. Aleksandrovsky, Maxim S. Molokeev, Aleksandr S. Oreshonkov, Victor V. Atuchin, Microwave synthesis and spectroscopic properties of ternary scheelite-type molybdate phosphors NaSrLa(MoO₄)₃: Er³⁺/Yb³⁺, J. Alloy. Comp. 713 (2017) 156–163.
- [64] C.S. Lim, A.S. Aleksandrovsky, M.S. Molokeev, A.S. Oreshonkov, D.A. Ikonnikov, V.V. Atuchin, Triple molybdate scheelite-type upconversion phosphor NaCa-La(MoO₄)₃:Er³⁺/Yb³⁺: structural and spectroscopic properties, Dalton Trans. 45 (2016) 15541–15551.
- [65] A.S. Oreshonkov, J.V. Gerasimova, A.A. Ershov, A.S. Krylov, K.A. Shaykhutdinov, A.N. Vtyrin, M.S. Molokeev, K.Y. Terent'ev, N.V. Mihashenok, Raman spectra and phase composition of MnGeO₃ crystals, J. Raman Spectrosc. 47 (2016) 531–536.
- [66] V.V. Atuchin, A.S. Aleksandrovsky, O.D. Chimitova, T.A. Gavrilova, A.S. Krylov, M.S. Molokeev, A.S. Oreshonkov, B.G. Bazarov, J.G. Bazarova, Synthesis and spectroscopic properties of monoclinic α -Eu₂(MoO₄)₃, J. Phys. Chem. C 118 (2014) 15404–15411.
- [67] Z. Xia, M.S. Molokeev, A.S. Oreshonkov, V.V. Atuchin, R.-S. Liu, C. Dong, Crystal and local structure refinement in Ca₂Al₃O₆F explored by X-ray diffraction and Raman spectroscopy, Phys. Chem. Chem. Phys. 16 (2014) 5952–5957.